machines

MDPI

Article

Yaw Control and Yaw Actuator Synchronised Control of Large Wind Energy Converters Using a Non-Linear PI Approach

Adrian Gambier

Institute for Wind Energy Systems, Leibniz University Hannover, Appelstr. 9A, 30167 Hannover, Germany; agambier@ieee.org or adrian.gambier@iwes.uni-hannover.de

Abstract

This contribution studies the control of the yaw motion of large wind turbines. Two aspects are considered: the first is maximising the energy conversion by yawing the rotor in accordance with the wind direction. The other aspect is synchronising the control of all yaw actuators, which are affixed to the yaw gear rim. In a first phase, P and PI controllers are used in all control loops. Later on, the yaw controller and the synchronisers are replaced with nonlinear PI (NPI) controllers. Moreover, all actuator position P controllers are changed using nonlinear P (NP) controllers. Simulation experiments are carried out on the NREL 5 MW reference wind turbines. The results are very promising.

Keywords: wind turbine control; yaw control; actuator synchronisation; nonlinear PI control

1. Introduction

Modern large wind energy converters are being developed today, including a yaw system, which permits the accomplishment of a variety of duties, for instance, such as yawing the machine out of the wind, slowly following the wind direction, or manipulating the wake steering in wind farm control. In recent years, the significance of yaw control has increased for both individual turbines [1] and a group of turbines in a wind farm working together in wake steering control [2–4]. A review about yaw control is available in [5].

Nowadays, there are many methods for yaw control. Various methods are based on direct measurements of wind direction. The most common is a wind vane [6]. However, it is very imprecise. More accuracy is provided via LiDAR [7,8] and radar measurement systems [1]. Despite the fact that they offer more precise information regarding the wind direction, they remain expensive to integrate into each machine as standard sensors.

For these reasons, other approaches prefer to use an estimation of the wind direction based on prediction models, which depends on historical data and a prediction method. Several approaches are available, e.g., Bayesian learning [9], the fuzzy method [10], and data mining [11]. Finally, there are methods that do not use wind direction information. For example, a rotor speed control loop is proposed in [12], and hill climb searching (HCS) control is utilised in [13–15]. On the other hand, yaw control is also applied to reduce loads [16–18].

The control signal provided via the yaw controller goes to the yaw actuator. On the other hand, very large machines require attaching several actuators to the yaw gear rim in order to complete the torque that is necessary to rotate the nacelle and the rotor. Although all of these actuators can belong to the same type and series, they have differences, which can produce torque disbalances around the gear rim. This work condition for the actuators can lead to the irregular and forced operation of the motors at different internal conditions,

check for updates

Academic Editor: Zafer Bingul

Received: 24 June 2025
Revised: 16 July 2025
Accepted: 21 July 2025
Published: 24 July 2025

Citation: Gambier, A. Yaw Control and Yaw Actuator Synchronised Control of Large Wind Energy Converters Using a Non-Linear PI Approach. *Machines* **2025**, *13*, 644. https://doi.org/10.3390/machines13080644

Copyright: © 2025 by the author. Licensee MDPI, Basel, Switzerland. This article is an open access article distributed under the terms and conditions of the Creative Commons Attribution (CC BY) license (https://creativecommons.org/licenses/by/4.0/).

as well as bearing and gear rim wear. Hence, the matter is a multimotor synchronous control problem [19–21]. This topic has recently been presented in [22] for pitch actuators, for which a particular approach to cross-coupled control [23,24] based on the studies described in [25–29] is used.

Most approaches for both yaw control and yaw actuator control employ controllers of type P or PI. Nevertheless, the standard control approaches become progressively insufficient for maintaining an acceptable degree of control performance due to the highly increasing complexity of wind turbines. Thus, an alternative is to implement P and PI controllers with gains that nonlinearly change (see, e.g., [30,31]). This concept, which is frequently known as NPID (nonlinear PID), has been effectively implemented in robotics. In the context of wind turbine control, it has been applied in [32] for collective pitch control.

The objective of the present work is to revisit the yaw control system incorporating NPI instead of PI control and to study actuator yaw control from a synchronous control viewpoint while also considering NP and NPI controllers. The intention is, on the one hand, to improve power production by optimally tracking the wind direction and, on the other hand, to improve actuators, the gear rim, and the yaw bearing care.

The work is organised as follows: Section 2 is devoted to introducing some control fundamentals, which are the basis for the proposed approaches. In Section 3, the yaw control problem is formulated, and the solution is based on NPI controllers. It is followed by the description of yaw actuator control in Section 4. The numerical application is developed in Section 5, and the results are summarised in Section 6. Finally, Section 7 is dedicated to drawing the conclusions.

2. Control System Background

2.1. Basic Nonlinear PID

The linear PID controller is well known, and it is supported by ample literature (see, e.g., [33,34]). It is shortly presented in the following for the sake of completeness and as a support for the introduction of the NPID.

There are several configurations and variants, but the most used includes reference weighting, the filtering of the derivative, and anti-windup, namely

$$U(s) = K_p[bR(s) - Y(s)] + \frac{1}{s}[K_i E(s) + K_a\,[\overline{U}(s) - U(s)]] + \frac{K_d\, s}{1 + T_d s}[f\, R(s) - Y(s)] \quad (1)$$

K_p, K_i, and K_d are the proportional, integral, and derivative gains, respectively. The parameter b is a weighting factor between 0 and 1 for the reference signals R. The derivative term has a first-order filter, whose time constant is T_d. In this term, the reference is also multiplied by a factor, f, that can be either zero or one in order to avoid large control amplitudes when the reference presents large and abrupt changes. In addition, the integrative part is provided via an anti-windup mechanism with the tracking-time constant $T_a = 1/K_a$ in order to avoid integrator saturation.

The simplest nonlinear PID controller (NPID) is a standard PID controller, where the proportional gain is replaced with a nonlinear function, $f(e)$, of the control error (see, e.g., [35,36]). The function f is usually described by

$$f(e) = K_0 + K_1[g(e) - 1] \quad (2)$$

where $1 \leq g(e) \leq 2$. Hence, the proportional gain is K_0 for $g(e) = 1$ and $K_0 + K_1$ for $g(e) = 2$. Moreover, the idea is that $g(e) = 1$ for $e = 0$, which corresponds to the standard PID controller, and $g(e) = 2$ for $e = \pm\infty$. Thus, the controller has a large gain when the control system is far away from the operating point, and the gain is gradually reduced as the system approaches

the operating point. There are several functions that satisfy the conditions imposed on g. The most common are, for instance, the hyperbolic secant function and the smooth sigmoidal function [35], whose implementation can be

$$g(e) = 2 \ - \text{sech}(K_2 e) \tag{3}$$

for the hyperbolic secant and

$$g(e) = 2 \ - \text{sigm}(K_2|e|) \tag{4}$$

for the sigmoidal function. The constant K_2 is used to adjust the variation rate of $f(e)$. Figure 1 shows an example of functions $f(e)$ and $g(e)$.

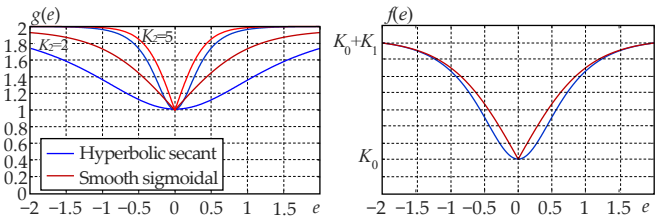


Figure 1. (**a**) Basic nonlinear function $g(e)$ with two different values of K_2. (**b**) Scaled nonlinear function $f(e)$.

This approach is limited because only the proportional gain is multiplied by the nonlinear function. However, all gains of the PID controller can individually be adjusted with a nonlinear function (see [37,38]).

2.2. Extended Nonlinear PID

More general nonlinear PID controllers are obtained by considering nonlinear functions for each controller gain. For instance, in [39], hyperbolic secant functions are used for each controller parameter, namely

$$f_p(e) = K_{0p} + K_{1p}[1 - \text{sech}(K_{2p}e)] \tag{5}$$

$$f_i(e) = 1/[K_{0i} + K_{1i}(1 - \text{sech}(K_{2i}e))], \text{and} \tag{6}$$

$$f_d(e) = 1/[K_{0d} + K_{1d}(1 - \text{sech}(K_{2d}e))] \tag{7}$$

In the present work, only NP and NPI are used, i.e., $f_d(e) = 0$, and the other gains are given by

$$f_p(e) = K_{0p} + K_{1p}[1 - \text{sech}(K_{2p}e)] \text{ and} \tag{8}$$

$$f_i(e) = K_{0i} + K_{1i}[1 - \text{sech}(K_{2i}e)] \tag{9}$$

Notice that, when $K_{2x} = 0$ (with x as p, i and d), the NPID controller becomes PID.

2.3. Synchronised Operation of Multiple Actuators

The problem of synchronising several pitch actuators has recently been treated in [22]. The topic has origins in the theoreticical works, which were first presented in [25–29]. The approach can be considered a particular case of the cross-coupled control method [23,24]. Methods for synchronous control are summarised and reviewed in, e.g., [21].

The case considered in this work includes a number of similar n actuators described using transfer functions $G_i(s) = B_i(s)/[s^{ni} A_i(s)]$ with Hurwitz denominators and $i = 1...n$,

whose output responses $y_i(t)$ approach distinct values for a common step input $U(s)$. Hence, the objective is to find a set of $(n-1)$ identical synchronisers, $H(s) = Q(s)/P(s)$, such that the outputs converge to the same value, i.e.,

$$y_1(t)|_{t\to\infty} = y_2(t)|_{t\to\infty} = \ldots = y_n(t)|_{t\to\infty} = u(t)|_{t\to\infty} \tag{10}$$

where the denominator $P(s)$ has the minimal order that is required to satisfy (8). The configuration for the synchronisation of four actuators is shown in Figure 2.

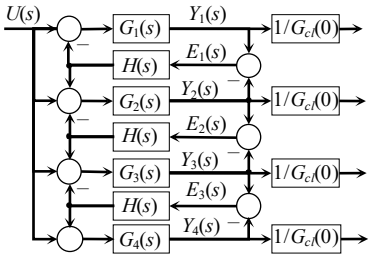


Figure 2. Synchronisation of four actuators.

The outputs are scaled by the closed-loop stationary gain $G_{cl}(0)$ in order to satisfy the conditions expressed in (11).

3. Yaw Control of Wind Turbines

In order to align the rotor with the wind direction, the yaw actuators are operated, causing the nacelle to turn around the vertical axis of the tower. This can be carried out if the wind direction is known, which can be obtained by means of a wind vane. The process of aligning the rotor with the wind direction is illustrated in Figure 3.

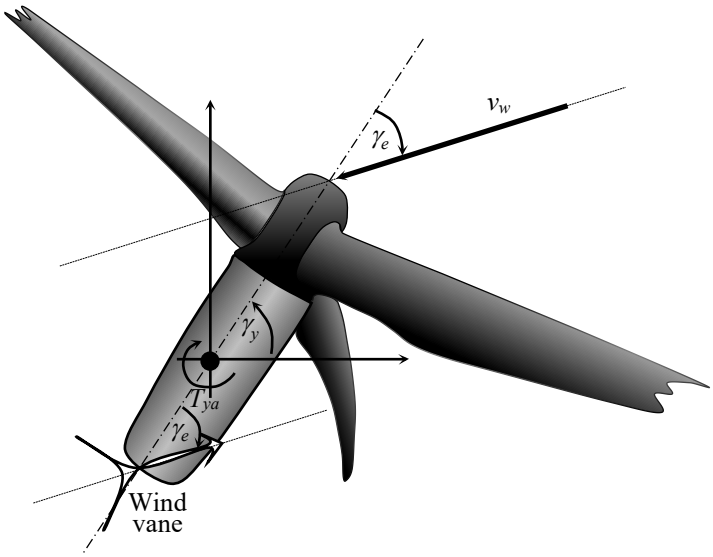


Figure 3. Yaw misalignment of a wind turbine.

A controller with a dead zone [40] is commonly utilised to implement a conventional yaw control loop. Due to the dead zone, the controller is only activated when the control error overflows the predetermined threshold given by the dead zone, and its purpose is to return the operation to the region [41]. As the reference to be tracked, a weighted averaged wind direction signal, $\overline{\gamma_e}$, is used, which is derived from a wind vane placed at the rear of the nacelle and a low-pass filter. The control system scheme is shown in Figure 4.

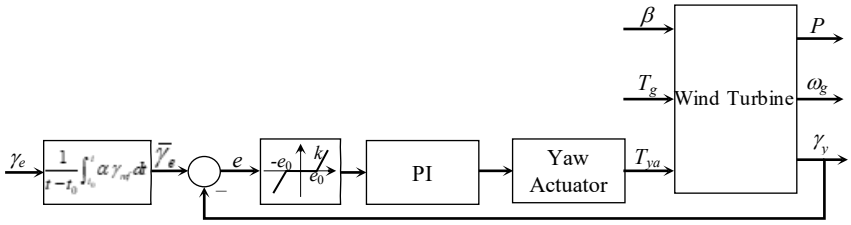


Figure 4. Scheme of a yaw control system with dead zone.

The controller is normally implemented as a PI control law, which becomes active when the control error exceeds the dead zone defined in the band $[-e_0, e_0]$ as

$$e_o(t) = \begin{cases} 0 & |e(t)| \leq |e_0| \\ k\, e(t) & |e(t)| > |e_0| \end{cases} \tag{11}$$

The measured output is the yaw angle γ_y (see Figure 3), such that the control error is $e = \overline{\gamma_e} - \gamma_y$.

The measurement of the wind direction is imprecise and noisy. Therefore, it is essentially inadequate to be used as a setpoint for the control system. Consequently, it is smoothed here by passing it through a moving average filter. However, continuously tracking the reference is unnecessary because the yaw mechanism operates very slowly. Hence, it can be activated only when the misalignment becomes noticeable. That is the duty of the dead zone.

As will be shown later in the practical study, a standard dead zone strongly reduces performance: if it is chosen large to reduce the yaw activity, the tracking is poor, reducing the energy conversion, and if it is small, shattering occurs around the reference. For this reason, an adaptive dead zone is implemented in this work, such that the zone is chosen small when the error is large to ensure that the output variable very closely resembles the reference and then changes to a larger zone to reduce the activity of the yaw mechanism once the output is near the reference.

Moreover, the performance of a standard yaw control system is also improved by replacing the classic PI with the NPI controller. The control law is then

$$u(t) \; = f_p[e(t)][b\, r(t) - y(t)] + \int_0^t \{f_i\,[e(t)]e(t) + K_a\,[\overline{u}(t) - u(t)\Big\} dt \tag{12}$$

where $\bar{u}(t)$ is the control signal after the actuator, which is used for the anti-windup mechanism, and f_p and f_i are the nonlinear functions defined by (8) and (9).

4. Yaw Actuator Control

4.1. Control System for an Individual Actuator

The control of an actuator based on PMSG is described in detail in [22]. The complete control system, which includes two PI current controllers with nonlinear feedforward terms, one PI speed controller with zero compensation, and a derivative feedforward-feedback controller, is shown in Figure 5.

The transfer function for the closed-loop system is then expressed by

$$\Theta_m(s) = \frac{(K_{p\theta} + K_{vff}s)B_s(s)}{s\, A_s(s) + B_s(s)K_{p\theta}}\; \Theta_{mref}(s) - \frac{B_T(s)}{s\, A_s(s) + B_s(s)K_{p\theta}} T_L(s) \tag{13}$$

$$B_s(s) = b_{m1}a_{i2}K_{i\omega},\; A_s(s) = s(s + a_{m1})(s^2 + a_{i1}\, s + a_{i2}) + b_{m1}a_{i2}(b\, K_{p\omega}\, s + K_{i\omega}) \text{ and } B_T(s) = b_{m1}\, s\, (s^2 + a_{i1}\, s + a_{i2}) \tag{14}$$

where $b_{m1} = 1/J_m$, $a_{m1} = B_m/J_m$, $a_{i1} = (R_s + K_{pq})/L_q$, and $a_{i2} = K_{iq}/L_q$. The parameters L_d, L_q, R_s, J_m, and B_m are inductances, resistance, the mass moment of inertia, and the viscous friction of the motor, respectively. The gains K_{pq}, $K_{\omega ff}$, K_{pw} K_{iw}, K_{pq}, and K_{iq} are the parameters of the different controllers. Notice that, in the case of the NP controller, the gain K_{pq} is variable with the control error.

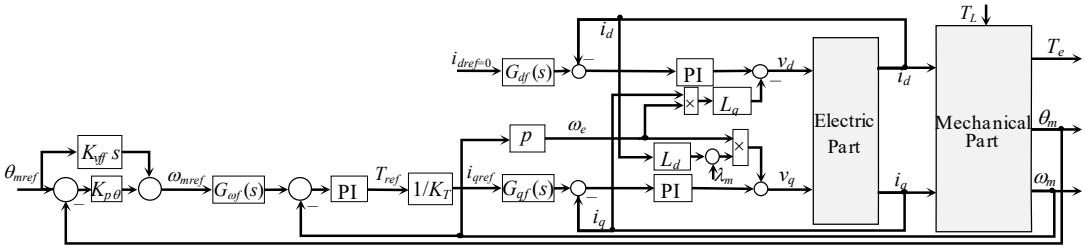


Figure 5. Block diagram of the actuator and its control system [22].

4.2. Synchronised Operation of Multiple Yaw Actuators

Since all actuators are attached to the same gear rim, the interest here is to synchronise the torques. Hence, the synchronisation for n actuators is carried out by means of $(n-1)$ identical NPI controllers according to (8), (9), and (12) but with a different parametrisation, namely

$$f_{ps}(e) = K_{0ps} + K_{1ps}[1 - \text{sech}(K_{2ps}e)]\text{and} \tag{15}$$

$$f_{is}(e) = K_{0is} + K_{1is}[1 - \text{sech}(K_{2is}e)] \tag{16}$$

The control system configuration is portrayed in Figure 6.

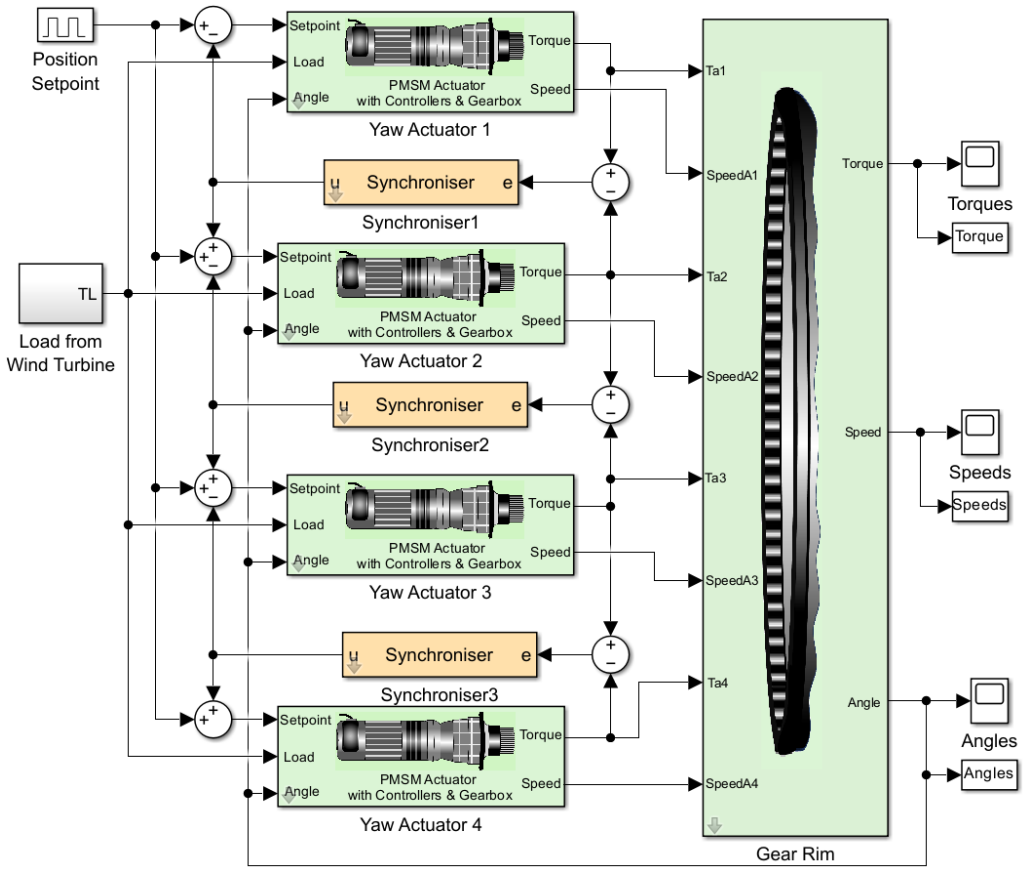


Figure 6. Block diagram of the synchronised actuator control system.

5. Application Study

5.1. Parametrisation of the Reference Wind Turbine

The wind turbine objective for the numerical study is the three-bladed 5-MW machine from NREL [42], whose maximum yaw load moment is estimated to be about T_g = 7833.7 kNm. The rotor has a diameter of 126 m and a hub height of 90 m. The tower top diameter is 3.87 m. The rated yaw speed is w_{gn} = 0.05 rpm.

Notice that the wind turbine has a high number of parameters and specifications; see [42] for a list of them.

5.2. Parametrisation of the Yaw Actuator Model

The specifications for the actuator are a yaw speed of w_g = 0.05 rpm, and the tower top diameter d_t = 3.87 m, which is considered the gear rim diameter. The pinion diameter is d_p = 0.16 m.

In comparison to the torque of commercial yaw actuators, the maximal load moment is highly exceeding such actuator torques. Therefore, it is necessary to implement several joint-working yaw actuators in order to manage the load torque. The link between the motor torque and the load torque is denoted as

$$T_\gamma = n_a n_m n_x T_m \tag{17}$$

The parameter n_a represents the number of necessary actuators, n_m symbolises the gear rim ratio, and n_x is the ratio of the gearbox. The gear rim ratio is obtained from $n_m = d_t/d_p = 3.87/0.16 = 24.2$. The gearbox ratio, n_x, can be computed as $w_m/(n_m w_g)$, where w_g and w_m are the yaw speed and the as motor speed, respectively. Under these definitions, (9) becomes

$$T_\gamma = \frac{n_a n_m \omega_m}{n_m \omega_\gamma} T_m = \frac{n_a \omega_m}{\omega_\gamma} T_m \tag{18}$$

A PMSM with six pole pairs, a torque of 102 Nm, and 960 rpm (100.531 rad/s) is selected for the yaw actuation. Hence, it follows that

$$n_x = \frac{\omega_m}{n_m \omega_\gamma} = \frac{960}{24.2 \;\; 0.05} = 793.4 \tag{19}$$

The required number of yaw actuators is

$$n_a = \frac{T_\gamma}{n_m n_x T_m} = \frac{7833700}{24.2 \;\; 793.4 \;\; 102} \simeq 4 \tag{20}$$

The attachment of four actuators to the gear rim is schematised in Figure 7.

In addition, the nominal values for line-to-line voltage are 230 V (v_{sd} = 96.3 V and v_{sq} = 208.9 V) and a current of 230.52 A (i_{sd} = 163 A and i_{sq} = 163 A). Moreover, the torque difference in the stationary state is defined as $DT = T_e - T_g/(n_a\, n_m\, n_x) = 0.1$. The steady-state equations in matrix form for the model are expressed as

$$\begin{bmatrix} L_d \\ R_s \\ \lambda_f \\ B_m \end{bmatrix} = \begin{bmatrix} -p\omega_m & i_{sd} & 0 & 0 \\ p\omega_m i_{sd} & i_{sq} & p\omega & 0 \\ 0 & 0 & 1.5 p i_{sq} & 0 \\ 0 & 0 & 0 & \omega_m \end{bmatrix}^{-1} \begin{bmatrix} v_{sd} \\ v_{sq} \\ T_m \\ \Delta T \end{bmatrix} \tag{21}$$

By solving (13) for p = 6, the physical parameters are $L_d = L_q = 0.359343 \times 10^{-3}$ H, R_s = 0.8045 Ω, λ_f = 0.07072 Wb, and B_m = 0.0147 Nm s/rad. The second moment of inertia is estimated by J_m = 1.6134 kg m^2, which completes the actuator parametrisation. The

parameters for the other three actuators are obtained by random parameter variation inside a band of 10% of the first one. All parameters are summarised in Table 1.

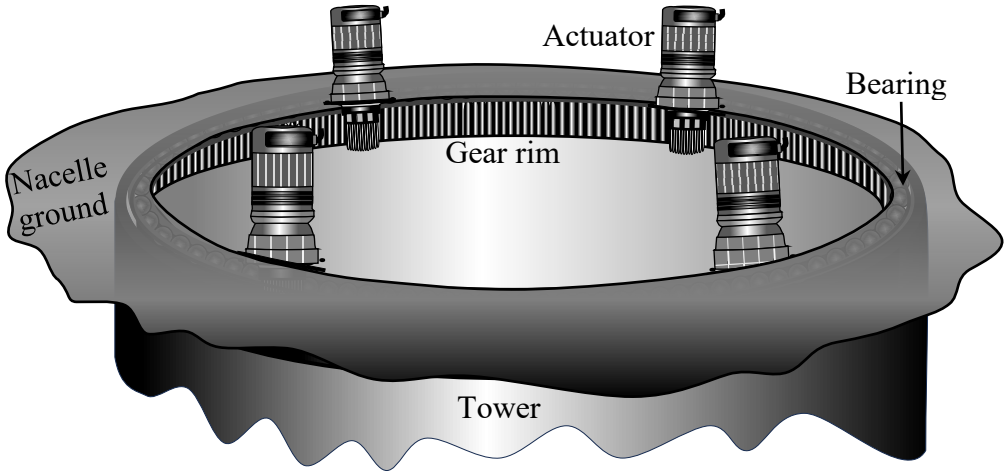


Figure 7. Simplified scheme of four actuators attached to the gear rim.

Table 1. Actuator parameters.

Parameters	Actuator 1	Actuator 2	Actuator 3	Actuator 4
J_m [kg m^2]	1.6134	1.5327	1.6457	1.6505
B_m [N m/(rad/s)]	0.0147	0.018919	0.0075661	0.009241
L_d [H]	0.00035934	0.00034138	0.00053901	0.00048511
L_q [H]	0.00035934	0.00034138	0.00053901	0.00048511
R_s [Ω]	0.80455	0.76432	1.2068	1.0861
l_f [Wb]	0.07072	0.068217	0.076378	0.076095
p	6	6	6	6

5.3. Control Systems and Controller Parametrisation

5.3.1. Control Loops and Controller Parameters for the Yaw System

The NPI controller is compared with a standard PI controller. Hence, controller parameters for both are obtained via the simulation-based numerical minimisation of the ITSE objective function (integral time-weighted squared error, see (22)) by using the active-set method under stability constraints, i.e., Hurwitz closed-loop poles. All parameters are summarised in Table 2.

Table 2. Parameters for the yaw controllers.

Parameters	Proportional Gain	Integral Gain	Actuator 3	Reference Weight
PI	$K_{py} = 7.372$	$K_{iy} = 3.443$	$K_{ay} = 5$	$b = 1$
NPI	$K_{0py} = 4.4173$ $K_{1py} = 8.6107$ $K_{2py} = 0.0143$	$K_{0iy} = 4.4173$ $K_{1iy} = 8.6107$ $K_{2iy} = 0.0143$	$K_{ay} = 5$	$b = 1$

5.3.2. Control Loops and Controller Parameters for the Yaw Actuators

As mentioned before, the design of the synchronisers requires the models of the considered plants, in this case, the actuators, which in turn have three levels of cascade control (current, speed, and position control). Thus, the controller parameters of all actuators are needed to design the synchronisers. They are designed individually by using the same

procedure as mentioned in the previous section. The simulation results of the separately and decoupled from gear rim controlled actuators are portrayed in Figure 8 for a P position controller and Figure 9 for an NP position controller. The controller parameters are summarised in Table 3.

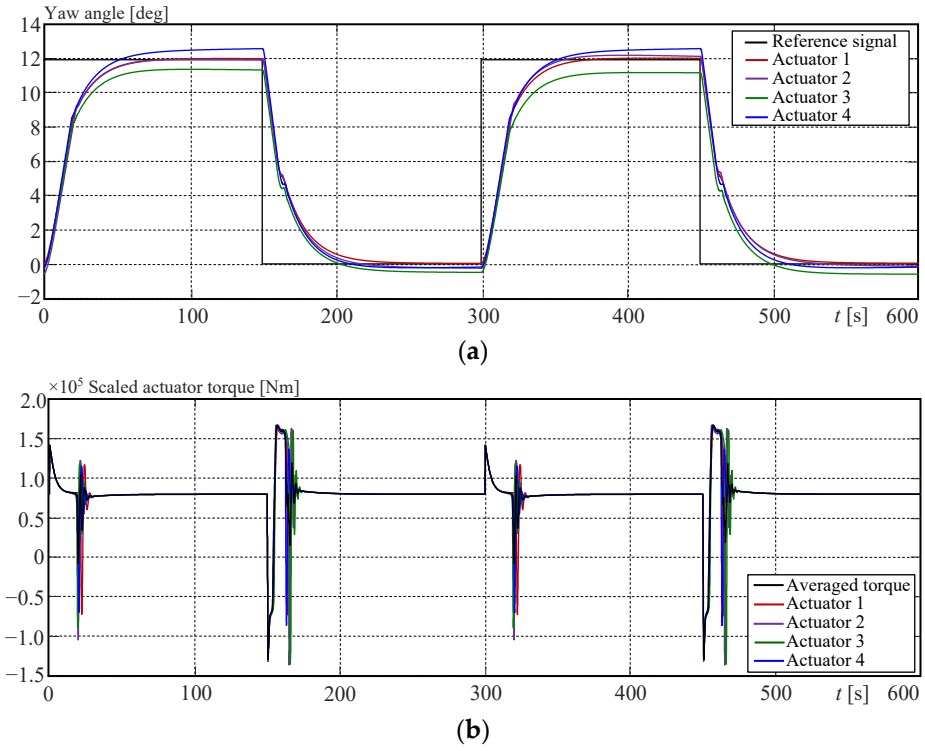


Figure 8. Angles (**a**) and torques (**b**) of each actuator separately with P position control.

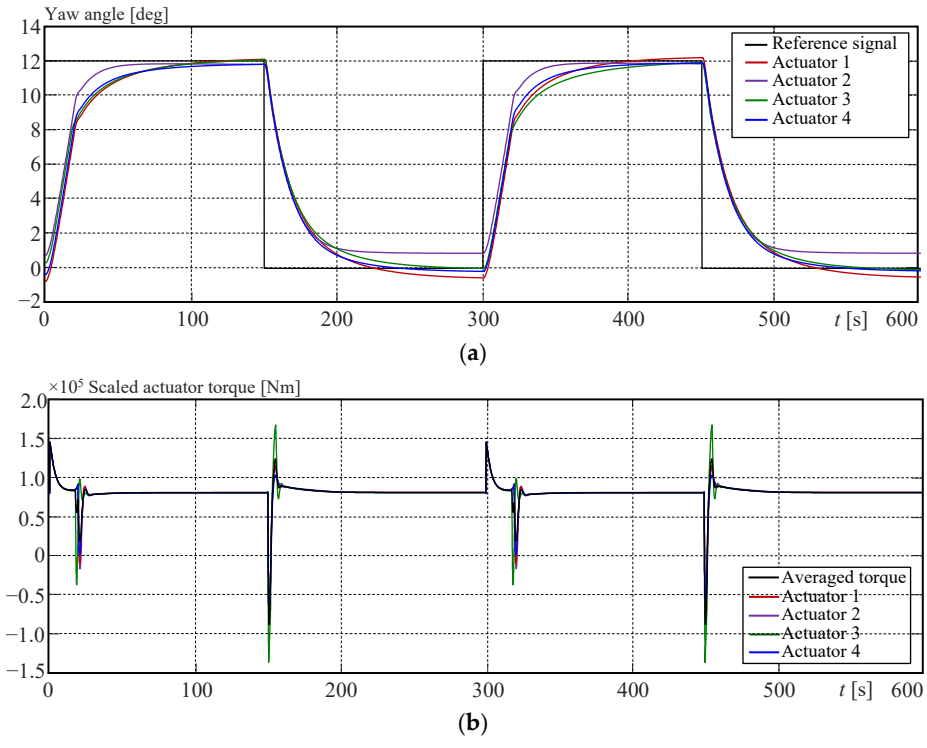


Figure 9. Angles (**a**) and torques (**b**) of each actuator separately with NP position control.

Table 3. Controller parameters of actuators.

Parameters		Actuator 1	Actuator 2	Actuator 3	Actuator 4
Current controllers		$K_{pd} = 0.0870$ $K_{id} = 0.1710$ $K_{pq} = 1.0489$ $K_{iq} = 2.5310$	$K_{pd} = 0.0870$ $K_{id} = 0.1710$ $K_{pq} = 1.0489$ $K_{iq} = 2.5310$	$K_{pd} = 0.0870$ $K_{id} = 0.1710$ $K_{pq} = 1.0489$ $K_{iq} = 2.5310$	$K_{pd} = 0.0870$ $K_{id} = 0.1710$ $K_{pq} = 1.0489$ $K_{iq} = 2.5310$
Speed controllers		$K_{pt} = 4.1952$ $K_{it} = 0.0290$	$K_{pt} = 1.5646$ $K_{it} = 0.0215$	$K_{pt} = 3.5038$ $K_{it} = 0.0192$	$K_{pt} = 5.7635$ $K_{it} = 0.0294$
Position controllers	FF	$K_{vff} = 20.6395$	$K_{vff} = 20.6395$	$K_{vff} = 22.2367$	$K_{vff} = 26.2889$
	P	$K_{pp} = 20.1020$	$K_{pp} = 20.2919$	$K_{pp} = 20.8031$	$K_{pp} = 20.3189$
	NP	$K_{pp1} = 15.4355$ $K_{pp2} = 2.3869$ $K_{pp3} = 1.0000$	$K_{pp1} = 1.2978$ $K_{pp2} = 16.4546$ $K_{pp3} = 1.0000$	$K_{pp1} = 12.6032$ $K_{pp2} = 5.0307$ $K_{pp3} = 1.0000$	$K_{pp1} = 9.8339$ $K_{pp2} = 8.0440$ $K_{pp3} = 1.0000$

The NP position control demonstrates superior performance compared to the P controllers, particularly in terms of output angles. Values of performance indices J_e (integral time-weighted squared error, ITSE, see (17)) are summarised in Table 4.

Table 4. Values of the performance index for all actuators without synchronisation.

	P Position Controller				NP Position Controller			
	Actuator 1	Actuator 2	Actuator 3	Actuator 4	Actuator 1	Actuator 2	Actuator 3	Actuator 4
J_e	685.5	543.5	743.4	564.5	211.4	480.6	598.5	559.3

5.4. Setup for the Simulation Environment

The wind turbine simulations take place in OpenFAST V4.1.0 from NREL (formerly known as FAST [43]). The wind speed is chosen to be stepwise with 5% turbulence in the x- and y-directions changing between 12 and 22 m/s (see Figure 10).

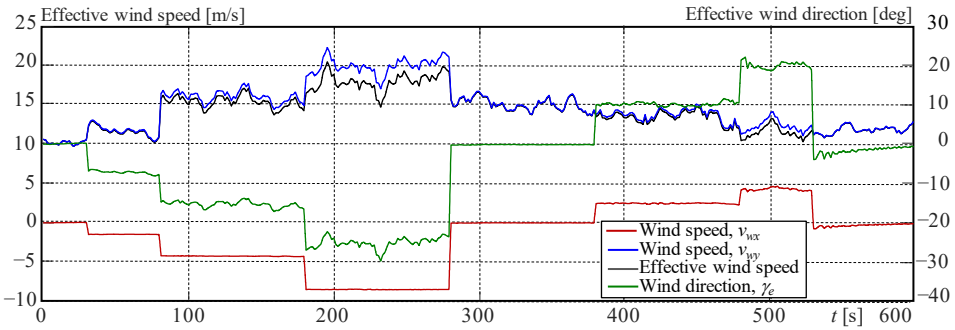


Figure 10. Wind profile used in the simulation experiments.

5.5. Description of the Simulation Experiments

The simulation experiments are divided into two groups. The first group is dedicated to the yaw control. Simulations are carried out for different dead zones and for the classic PI, as well as the NPI controllers. For the comparison, three objective functions are evaluated, namely

$$J_e = \frac{1}{t_f - t_i}\int_{t_i}^{t_f} t\,[e_\gamma(t)/e_{\gamma max}]^2 dt,\; J_u = \frac{1}{t_f - t_i}\int_{t_i}^{t_f} t\,[u(t)/u_{max}]^2 dt, \text{ and } E = \frac{1}{3600}\int_{t_i}^{t_f} t\,P_e(t)\,dt \tag{22}$$

J_e and J_u are the averaged integral of time-weighted squared control error (ITSE) and of the squared control signal (ITSU), respectively. The last one, E, is the average energy converted, expressed in kWh. While in the first two functions, smaller numbers indicate

better performance, in the third one, the improvement in performance is characterised by an increase in the value of converted energy.

The second group of experiments is devoted to the synchronisation of yaw actuators, also considering PI, as well as NPI controllers as synchronisers. The objective functions are evaluated in this case considering the differences between the output torques of the actuators.

6. Simulation Results and Analysis

6.1. Simulation Results for the Yaw Control Experiment

First, the performances of PI and NPI controllers without a dead zone are compared. As a reference signal to be tracked, the moving-averaged filtered wind direction is used. The results are shown in Figure 11.

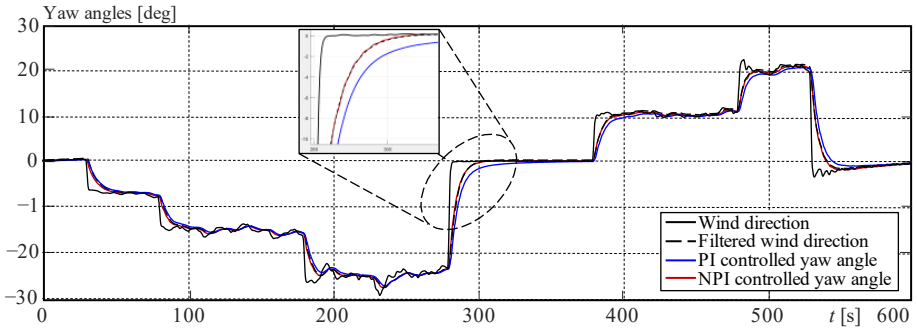


Figure 11. Controlled yaw angles using PI, as well as NPI controllers.

It is possible to observe that the NPI shows a practically perfect tracking performance while the PI controller is a bit inferior. The quantitative comparison indicates $J_e = 0.3566$ for the PI controller and $J_e = 0.0071$ for the NPI. The energy conversion E is also slightly better for the NPI (262.8 against 262.0), and both have practically the same control activity $J_u = 68.594$.

The second experiment consists of testing the yaw control system for different dead zones. Yaw mechanisms are normally not designed for continuous operation. The necessary inactivity is implemented by a dead zone, where inactivity time is given by the width of the dead zone. During the inactivity, the yaw angle can drift away from the reference. Therefore, the performance of the wind turbine will deteriorate in the time that the yaw mechanism is inactive. Thus, the aim of this test is to find a compromise between reduced deteriorated performance and reduced yaw activity. This is studied by testing different dead zones. The simulation results are presented in Figure 12.

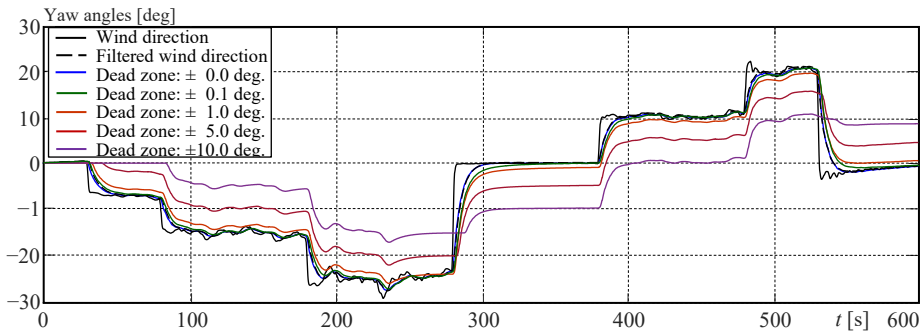


Figure 12. NPI control results for different dead zones.

The curves show the tracked yaw angles regarding the reference (dashed curve). The control errors are given by the distance between the curve corresponding to the considered

dead zone and the reference. It is clear that the control errors increase with the increasing width of the dead zone.

The quantitative analysis summarised in Table 5 indicates that the PI controller with a dead zone of ±5.0 deg yields the minimum actuator activity (J_u = 62.3505), but, on the other hand, the energy conversion is reduced (E = 256.1) and the tracking performance is poor (J_e = 17.6656). Notice that the NPI with a dead zone ±1.0 deg has a comparable actuator activity (J_u = 65.6015) but achieves good tracking performance (J_e = 1.2507) and energy conversion (E = 262.8).

Table 5. Values of performance indices for PI and NPI controllers with different dead zones.

Dead Zone	PI			NPI		
	J_e	J_u	E	J_e	J_u	E
0 deg	0.3566	68.5939	262.0	0.0071	68.5942	262.8
±0.1 deg	0.4182	69.1778	262.0	0.0269	68.9010	263.0
±1.0 deg	1.2507	68.1147	261.4	0.4072	65.6015	262.8
±5.0 deg	17.6656	62.3505	256.1	6.8705	78.0999	258.2
±10.0 deg	100.9248	73.2117	242.0	26.3100	77.2117	252.7
Adaptive: (±0.2, ±15.0) deg	0.4775	69.1624	261.9	0.0380	69.4918	261.9
Adaptive: (±0.1, ±15.0) deg	0.4009	69.2013	262.0	0.0290	68.8906	262.0

In the last experiment, the yaw control system is implemented with the adaptive dead zone, considering two cases. In the first one, the dead zone width changes from ±15.0 to ±0.2 degrees, and in the last one, the change is between ±15.0 and ±0.1 degrees. The results are depicted in Figure 13 compared with the best case of fixed dead zones.

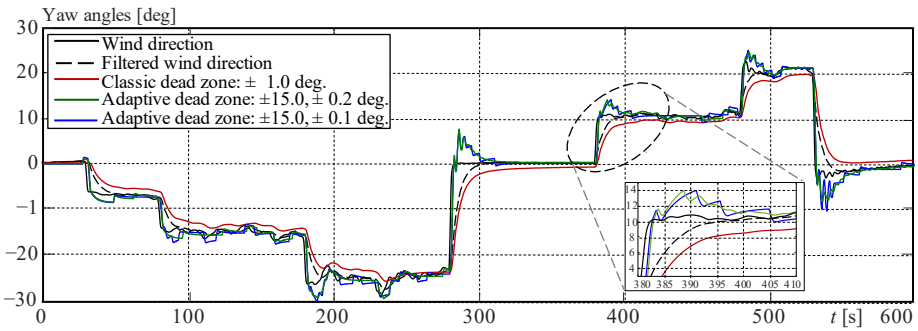


Figure 13. NPI control with adaptive dead zones.

The idea of the adaptive dead zone is to improve the tracking performance without a significant increment in actuator activity.

Finally, all results regarding the quantitative study are summarised in Table 5.

6.2. Simulation Results for the Yaw Actuator Control Experiment

The yaw actuator control was first implemented by using PI control for the current and speed controllers and a P controller for the position, following the classic approach [44]. The synchronisers were also implemented as PI controllers. Later, all position controllers and the synchronisers were changed to NP and NPI control laws.

Since all actuators are attached to the same gear rim, balanced torque distribution is an essential aspect, but the angles are also synchronised because of mechanical constraints.

The synchronised control with PI controllers is shown in Figure 14, and with NPI controllers in Figure 15.

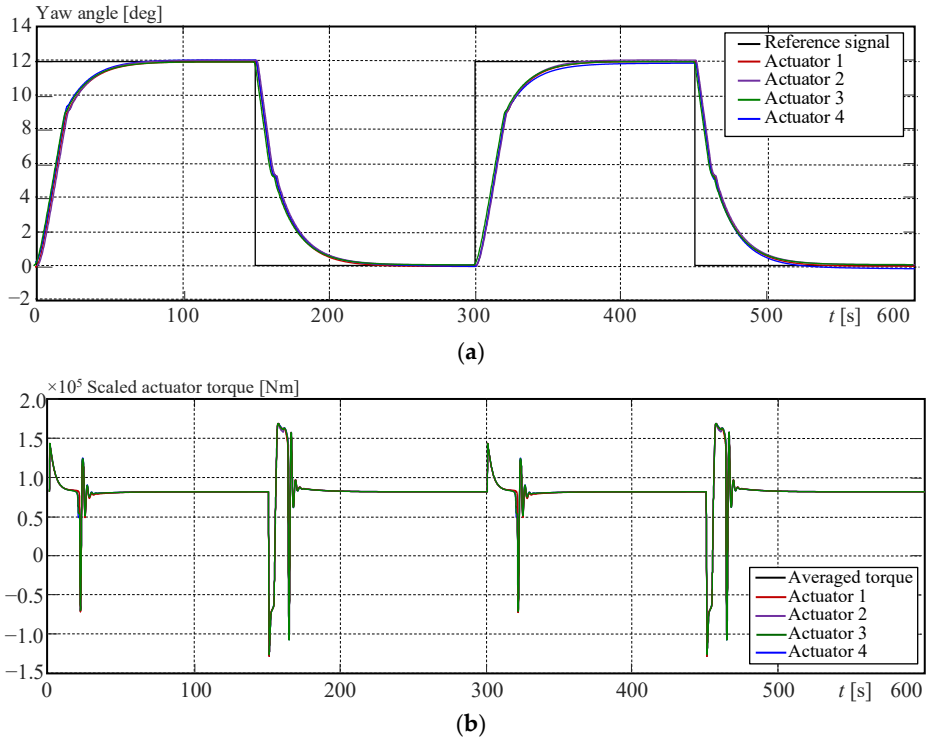


Figure 14. Angles (**a**) and torques (**b**) for the synchronised actuator control with PI controllers.

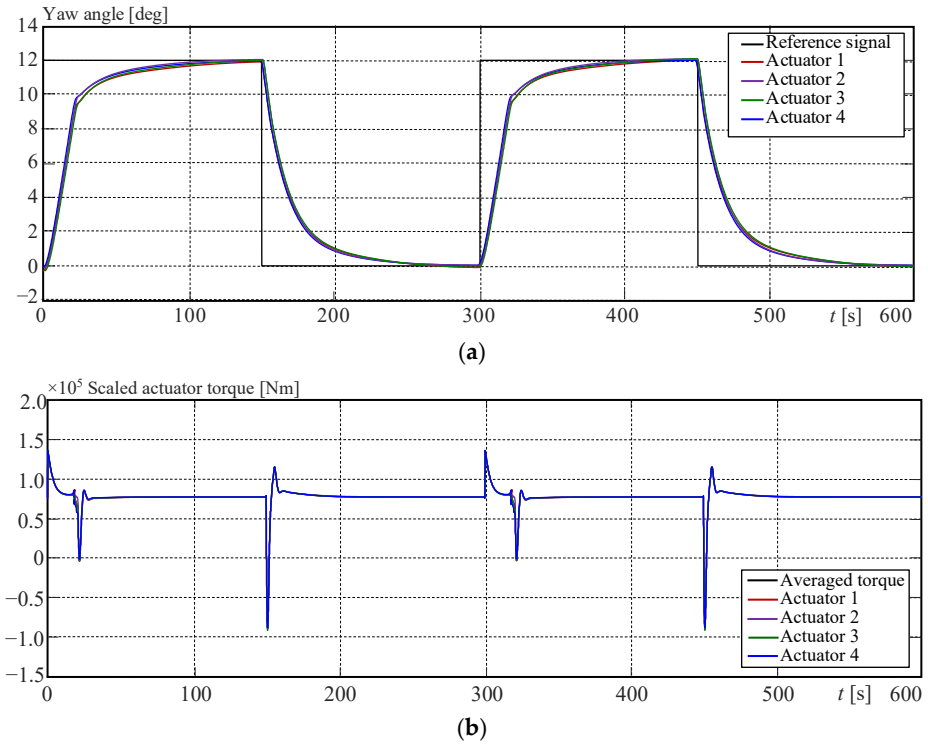


Figure 15. Angles (**a**) and torques (**b**) with NPI synchronisers.

The results of the computed performance indices are expressed in Table 6.

When Tables 5 and 6 are compared, it is clear that the synchronisation provides an important improvement regarding the non-synchronised approach. Moreover, NPI synchronisers also present an improved performance with respect to the PI controllers.

Table 6. Values of the performance index for all actuators with synchronisation.

	PI Synchronisers				**NPI Synchronisers**			
	Actuator 1	Actuator 2	Actuator 3	Actuator 4	Actuator 1	Actuator 2	Actuator 3	Actuator 4
J_e	206.03	432.01	151.09	154.91	30.20	47.85	45.23	95.73

7. Conclusions

This study has been devoted to investigating the problem of tracking the wind direction of large wind energy converters, which is known as yaw control. Two aspects were considered. The first one was the yaw control problem itself, considering dead zones in order to reduce the actuator activity. The second aspect concerns the necessity of several actuators attached to the same gear rim to move the rotor and nacelle, which makes the synchronisation of these actuators important.

Yaw control is normally implemented using PI controllers. The synchronisation of yaw actuators is actually a new topic, but synchronisers can also be implemented with PI control laws. In order to improve the control performance regarding the tracking of the wind direction, the use of nonlinear P and PI controllers was explored.

The experiments were conducted on the NREL 5 MW reference wind turbine, which was implemented in OpenFAST. For the control system, MATLAB®/Simulink (R2024a) were utilised. The simulation results were evaluated qualitatively according to the portrayed curves and quantitatively by using performance indices.

In general, NPI controllers showed the best performance in all cases. Moreover, the yaw control with an adaptive dead zone offers a better balance between actuator activity and power reduction due to misalignment, which is an advantage in the farm control application. The most important inconvenience in the case of yaw control is the inaccurate measurement or estimation of the wind direction. Hence, this aspect will be deeply studied in future work.

Concerning the actuator synchronisation problem, there are several possible research lines. The case of many actuators is one of the most important to be studied. For instance, about 16 yaw actuators are necessary for a 12 MW wind turbine [45], whose synchronisation can be very challenging.

Funding: This research received no external funding.

Data Availability Statement: Data are available upon request from the corresponding author if allowed by the affiliated institution.

Conflicts of Interest: The author declares no conflicts of interest.

Abbreviations

HCS	Hill climb searching
ISE	Integral square error
ITSE	Integral time-weighted squared error
ITSU	Integral time-weighted squared control
LiDAR	Light detection and ranging
NREL	National Renewable Energy Laboratory
PMSG	Permanent magnet synchronous motor
P, PI, PID	Proportional, proportional–integral, proportional–integral–derivative control
NP, NPI, NPID	Nonlinear P, nonlinear PI, nonlinear PID control

Nomenclature

Parameters	
a_i, b_i, p_i, q_i	Elements of polynomials $A(s)$, $B(s)$, $P(s)$, $Q(s)$
B_m	Torsional viscous friction of motor shaft, Nm s/rad
J_m	Second moment of inertia of motor, kg m^2
K_{pq}, K_{vff},	Parameters of the position control
K_{pd}, K_{id}, K_{id}, K_{iq},	Gains of the current controllers (d and q axis)
K_{pw}, K_{iw}	Gains of the speed controller
K_0, K_1, K_2	Gains for the nonlinear controllers
K_p, K_i, K_d, K_a, b, f	Parameters of P, PI, PID controllers
L_d L_q	Self-inductances, H
n_a	Number of actuators
n_x, n_m	Gearbox and gear rim ratios, --
p	Number of pole pairs, --
d_p	Pinion diameter, m
d_t	Tower top diameter, m
R_s	Stator resistance, Ohm
T_{Lmax}	Maximum load torque, Nm
λ_f	Flux linkage between rotor and stator
w_{gn}	Rated yaw speed
Variables	Flapwise root bending moments
i_{sd}, i_{sq}	d and q currents, in the dq reference frame, A
i_{dref}, i_{qref}	d and q reference currents, in the dq reference frame, A
s	Laplace variable
t	Time
T_g	Yaw torque, Nm
T_L	Load torque, Nm
u	Control variable
y	Output variable
v_a, v_b, v_c	Three-phase input voltages, V
v_d, v_q	d and q input voltages, in the dq reference frame, V
v_{we}	Effective wind speed
g_e, g_y,	Yaw error angle and yaw angle, rad
w_e, w_m, w_g	Electric, mechanical, and yaw speeds, rad/s
Q_m, Q_{mref}	Laplace transform of angle and angle reference, rad
Functions	
$A_i(s)$, $A_s(s)$	Denominators of transfer function
$B_i(s)$, $B_s(s)$, $B_T(s)$	Numerators of transfer functions
$f(e)$, $g(e)$	Nonlinear function of the nonlinear PID controllers
$G_1(s)$, $G_2(s)$, $G_3(s)$, $G_4(s)$	Transfer functions
$G_{df}(s)$, $G_{dq}(s)$	Transfer functions of filters in the d and q axis
$H(s)$	Transfer function of the synchroniser
$Q(s)$, $P(s)$,	Numerator and denominator of controller or Synchroniser
$I_d(s)$, $I_q(s)$, $I_{dref}(s)$, $I_{qref}(s)$	Laplace transformed currents and current references
$U(s)$, $E(s)$, $Y(s)$, $R(s)$,	Laplace transformed input, error, output and reference
$W_m(s)$,$Q_m(s)$,$W_{mref}(s)$, $Q_{mref}(s)$	Laplace transformation of w_m, q_m, w_{mref}, q_{mref}

References

1. Liu, Y.; Liu, S.; Zhang, L.; Cao, F.; Wang, L. Optimization of the yaw control error of wind turbines. *Front. Energy Res.* **2021**, *9*, 626681. [CrossRef]
2. Bastankhaha, M.; Porté-Agelb, F. Wind farm power optimization via yaw angle control: A wind tunnel study. *J. Renew. Sustain. Energy* **2019**, *11*, 023301. [CrossRef]
3. Howland, M.F.; Lele, S.K.; Dabiria, J.O. Wind farm power optimization through wake steering. *Proc. Natl. Acad. Sci. USA* **2019**, *116*, 14495–14500. [CrossRef] [PubMed]
4. Knudsen, T.; Bak, T.; Svenstrup, M. Survey of wind farm control—Power and fatigue optimization. *Wind Energy* **2015**, *18*, 1333–1351. [CrossRef]
5. Yang, J.; Fang, L.; Song, D.; Su, M.; Yang, X.; Huang, L.; Joo, Y.H. Review of control strategy of large horizontal-axis wind turbines yaw system. *Wind Energy* **2021**, *24*, 97–115. [CrossRef]
6. Song, D.; Yang, J.; Fan, X.; Liu, Y.; Liu, A.; Chen, G.; Joo, Y.H. Maximum power extraction for wind turbines through a novel yaw control solution using predicted wind directions. *Energy Convers. Manag.* **2018**, *157*, 587–599. [CrossRef]
7. Chen, W.; Liu, H.; Lin, Y.; Li, W.; Sun, Y.; Zhang, D. LSTM-NN yaw control of wind turbines based on upstreamWind information. *Energies* **2020**, *13*, 1482. [CrossRef]
8. Fleming, P.A.; Scholbrock, A.K.; Jehu, A.; Davoust, S.; Osler, E.; Wright, A.D.; Clifton, A. Field-test results using a nacelle-mounted lidar for improving wind turbine power capture by reducing yaw misalignment. *J. Phys. Conf. Ser.* **2014**, *524*, 012002. [CrossRef]
9. Yang, M.; Fan, S.; Lee, W.J. Probabilistic short-term wind power forecast using componential sparse Bayesian learning. *IEEE Trans. Ind. Appl.* **2013**, *49*, 2783–2792. [CrossRef]
10. Kavousi-Fard, A.; Khosravi, A.; Nahavandi, S. A new fuzzy-based combined prediction interval for wind power forecasting. *IEEE Trans. Power Syst.* **2016**, *31*, 18–26. [CrossRef]
11. Ouyang, T.; Kusiak, A.; He, Y. Predictive model of yaw error in a wind turbine. *Energy* **2017**, *123*, 119–130. [CrossRef]
12. Karakasis, N.; Mesemanolis, A.; Nalmpantis, T.; Mademlis, C. Active yaw control in a horizontal axis wind system without requiring wind direction measurement. *IET Renew. Power Gener.* **2016**, *10*, 1441–1449. [CrossRef]
13. Guo, F.; Jiang, W.; Shao, H.; Du, Y.; She, J. Research on the wind turbine yaw system based on PLC. In Proceedings of the 29th Chinese Control and Decision Conference (CCDC), Chongqing, China, 28–30 May 2017; pp. 5164–5168.
14. Farret, F.A.; Pfitscher, L.L.; Bernardon, D.P. Sensorless active yaw control for wind turbines. In Proceedings of the 27th Annual Conference of the IEEE Industrial Electronics Society, Denver, CO, USA, 29 November–2 December 2001; pp. 1370–1375. [CrossRef]
15. Wu, X.; Liu, Y.; Teng, W. Modified hill climbing method for active yaw control in wind turbine. In Proceedings of the 31st Chinese Control Conference, Hefei, China, 25–27 July 2012; pp. 6677–6680.
16. Ekelund, T. Yaw control for reduction of structural dynamic loads in wind turbines. *J. Wind. Eng. Ind. Aerodyn.* **2000**, *85*, 241–262. [CrossRef]
17. Hure, N.; Turnar, R.; Vasak, M.; Bencic, G. Optimal wind turbine yaw control supported with very short-term wind predictions. In Proceedings of the IEEE International Conference on Industrial Technology (ICIT), Seville, Spain, 17–19 March 2015; pp. 385–391. [CrossRef]
18. Kragh, K.A.; Hansen, M.H. Load alleviation of wind turbines by yaw misalignment. *Wind Energy* **2014**, *17*, 971–982. [CrossRef]
19. Hu, S.; Ren, X.; Zhao, W. Synchronous control of multi-motor driving servo systems. In *Lecture Notes in Electrical Engineering*; Jia, Y., Du, J., Zhang, W., Eds.; Springer: Singapore, 2017; Volume 459, pp. 611–620. [CrossRef]
20. Li, M.; Meng, X. Analysis and design of system for multi-motor synchronous control. In *Advances in Computer Science, Environment, Ecoinformatics, and Education*; Lin, S., Huang, X., Eds.; Springer: Berlin/Heidelberg, Germany, 2011; Volume 217, pp. 268–273. [CrossRef]
21. Niu, F.; Sun, K.; Huang, S.; Hu, Y.; Liang, D. A review on multimotor synchronous control methods. *IEEE Trans. Transp. Electrif.* **2023**, *9*, 22–33. [CrossRef]
22. Gambier, A. Synchronised control of multiple actuators of wind turbines. *Actuators* **2025**, *14*, 264. [CrossRef]
23. Koren, Y. Cross-coupled biaxial computer control for manufacturing systems. *J. Dyn. Syst. Meas. Control* **1980**, *102*, 265–271. [CrossRef]
24. Zhao, D.; Li, C.; Ren, J. Speed synchronization of multiple induction motors with adjacent cross coupling control. In Proceedings of the 48h IEEE Conference on Decision and Control (CDC), Shanghai, China, 15–18 December 2009; pp. 6805–6810. [CrossRef]
25. Unbehauen, H.; Vakilzadeh, I. Synchronization of n non-identical simple-integral plants. *Int. J. Control* **1989**, *50*, 543–574. [CrossRef]
26. Vakilzadeh, I.; Mansour, M. Synchronization of 'n' integral-plus-times constant plants with non-identical gain and time constants. *Control Theory Adv. Technol.* **1989**, *5*, 569–585. [CrossRef]
27. Vakilzadeh, I.; Mansour, M. Synchronization of 'n" integral-plus-double time constant plants with non-identical gain and time constants. *J. FrankIm. Inst.* **1990**, *327*, 579–593. [CrossRef]

28. Unbehauen, H.; Vakilzadeh, I. Synchronization of 'n' decentralized non-identical plants with integral behavior and two complex poles. *Control Theory Adv. Technol.* **1994**, *10*, 385–402.
29. Vakilzadeh, I.; Unbehauen, H. Four rendezvous problems for n non-identical simple-integral plants. *Int. J. Syst. Sci.* **1993**, *24*, 1455–1472. [CrossRef]
30. Shahruz, S.M.; Schwartz, A.L. Design of optimal nonlinear PI compensators. In Proceedings of the 32nd IEEE Conference on Decision and Control, San Antonio, TX, USA, 15–17 December 1993; pp. 3564–3565.
31. Xu, Y.; Hollerbach, J.M.; Ma, D. A nonlinear PD controller for force and contact transient control. *IEEE Control Syst. Mag.* **1995**, *15*, 15–21.
32. Gambier, A.; Nazaruddin, Y. Collective pitch control with active tower damping of a wind turbine by using a nonlinear PID approach. *IFAC* **2018**, *51*, 238–243. [CrossRef]
33. Åström, K.J.; Hagglund, T. *Advanced PID control, ISA-The Instrumentation, Systems, and Automation Society*; Research Tringle Park: Durham, NC, USA, 2006.
34. Visioli, A. *Practical PID Control*; Springer: London, UK, 2006.
35. Seraji, H. A new class of nonlinear PID controllers with Robotic Applications. *J. Robot. Syst.* **1998**, *15*, 161–181. [CrossRef]
36. Su, Y.X.; Sun, D.; Duan, B.Y. Design of an enhanced nonlinear PID controller. *Mechatronics* **2005**, *15*, 1005–1024. [CrossRef]
37. Taylor, J.H.; Strobel, K.L. Nonlinear compensator synthesis via sinusoidal-input describing functions. In Proceedings of the 1985 American Control Conference, Boston, MA, USA, 19–21 June 1985; pp. 1242–1247.
38. Isayed, B.M.; Hawwa, M.A. A nonlinear PID control scheme for hard disk drive servosystems. In Proceedings of the 15th Mediterranean Conference on Control and Automation, Athens, Grecce, 27–29 June 2007; pp. 1–6. [CrossRef]
39. Junoh, S.C.K.; Salim, S.N.S.; Abdullah, L.; Anang, N.A.; Chiew, T.H.; Retas, Z. Nonlinear PID triple hyperbolic controller. *Int. J. Mech. Mechatron. Eng. Des. XY Table Ball-Screw Drive Syst.* **2017**, *17*, 1–10.
40. Slotine, J.-J.; Li, W. *Applied Nonlinear Control*; Prentice Hall, Englewood Cliffs: New Jersey, NJ, USA, 1991.
41. Burton, T.; Jenkins, N.; Sharpe, D.; Bossanyi, E. *Wind Energy Handbook Edition*, 2nd ed.; John Wiley and Sons: Chichester, UK, 2011.
42. Jonkman, J.; Butterfield, S.; Musial, W.; Scot, G. *Definition of a 5-MW Reference Wind Turbine for Offshore System Development. Technical Report*; NREL: Golden, CO, USA, 2009.
43. Jonkman, J.M.; Buhl Jr, L.M. *FAST User's Guide*; Research report, NREL; Battelle: Golden, CO, USA, 2005.
44. Wang, L.; Chai, S.; Yoo, D.; Gan, L.; Ng, K. *PID and Predictive Control of Electrical Drives and Power Converters Using MATLAB®/Simulink®*; John Wiley & Sons: Singapore, 2015.
45. Bonfiglioli. *Wind Solutions: Product Range. Product Description*; Bonfiglioli Riduttori S.p.A.: Carpiano, Italy, 2020.

Disclaimer/Publisher's Note: The statements, opinions and data contained in all publications are solely those of the individual author(s) and contributor(s) and not of MDPI and/or the editor(s). MDPI and/or the editor(s) disclaim responsibility for any injury to people or property resulting from any ideas, methods, instructions or products referred to in the content.